Power Electronics and Drives

Active Current Sensor Fault-Tolerant Control of Induction Motor Drive with Online Neural Network-Based Rotor and Stator Resistance Estimation

Michal Adamczyk*[iD], Teresa Orlowska-Kowalska[iD]

Department of Electrical Machines, Drives and Measurements, Wroclaw University of Science and Technology, Wroclaw, Poland

Abstract: This article presents an active current sensor (CS) fault-tolerant control (FTC) strategy for induction motor (IM) drive with adaptation of rotor and stator resistances. The stator current estimator with online adaptation of resistance parameters was applied for the reconstruction of missing current signals. A model reference adaptive system (MRAS), based on a neural network (NN), was used to estimate the rotor resistance. Additionally, stator resistance estimation was applied based on ratio index. The use of such a solution allowed for a significant increase in the quality of stator current reconstruction, which is particularly important for the design of CS fault detection (FD) and compensation algorithms. A wide range of simulation studies have been carried out for different operating conditions of the IM drive. The results showed that applying rotor and stator resistance estimation can improve the quality of stator current estimation by up to approximately 95% under rated operating point. The study was carried out for nominal and low speeds, with two, one, and without healthy CS.

Keywords: induction motor • fault-tolerant control • current sensor • resistances adaptation • neural network

Nomenclature

State variables:

$\mathbf{u}_s$	Spatial vector of stator voltage
$\mathbf{i}_s$, $\mathbf{i}_r$	Spatial vectors of stator and rotor currents
Ψ_s, Ψ_r	Spatial vectors of stator and rotor fluxes
t_{em}, t_L	Electromagnetic and load torques
ω_m	Angular rotor speed

Parameters:

r_s, r_r	Stator and rotor resistances
$l_{\sigma s}$, $l_{\sigma r}$, l_m	Stator and rotor leakage inductances and main inductance
T_M	Mechanical time constant
f_{sN}	Nominal frequency

1. Introduction

Induction motors (IMs) are among the largest group of electricity consumers due to their simple construction, ease of operation, and relatively low price compared with other types of motors. Therefore, they are widely used in industrial

* Email: michal.adamczyk@pwr.edu.pl

technological processes and recently in electrical transportation systems. To ensure the highest possible quality of operation, vector control methods must be used, which require stator current measurement. The determination of its value can be obtained by using LEM-type current sensors (CSs). Over time, the performance of electrical components deteriorates as a result of wear and ageing processes, reducing the reliability of the entire drive and process system and also increasing the risk of failure of basic system components. In practical applications, CS faults are among the most frequent failures (Shi and Krishnamurthy, 2014). Therefore, various concepts of CS fault-tolerant control (CS-FTC) systems can be found in the literature, which maintain the functionality of the electric drive despite the failure of CSs (Adamczyk and Orlowska-Kowalska, 2021; Azzoug et al., 2021; Najafabadi et al., 2010; Salmasi, 2017).

CS-FTC can be realised by two strategies: hardware and software redundancy. In this first group, additional sensors, actuators, or motors are used. In a situation when one of the three CSs is faulty, the other two can be used (Jankowska and Dybkowski, 2022). However, it should be noted that the use of additional components increases the cost of the drive system (Najafabadi et al., 2010). In the second group, algorithmic solutions are applied. When some CS is faulty, mathematical models are used to estimate the stator current (Adamczyk and Orlowska-Kowalska, 2019; Azzoug et al., 2021). However, these mathematical model-based methods are sensitive to changes in IM parameters, in particular rotor resistance. Additionally, in the low angular velocity range, the influence of stator resistance also becomes apparent (Adamczyk and Orlowska-Kowalska, 2022). Therefore, it is necessary to provide estimates of these parameters.

The resistance of the rotor can change by up to 50% during drive operation due to rotor heating. Obtaining this information using a thermal model or temperature sensor can be difficult. In the literature, the methods of estimation of selected parameters of IM are divided into two groups: working online and offline (Toliyat et al., 2003).

The first group, namely the offline methods, allow the parameters of the IM to be determined with a certain accuracy. However, they have limitations that result from the fact that they assume that the identified parameters remain unchanged in the entire operating range of the electric drive. Therefore, they do not provide precise solutions under drive operation. These techniques are mainly used in situations in which the system consists of components from different manufacturers.

Much more precise values are obtained with the use of online estimation methods. Due to the very large number and variety of such solutions, these methods were divided into four additional subgroups: methods using spectral analysis, techniques based on state observers, model reference adaptive system (MRAS) estimators, and other solutions (Toliyat et al., 2003).

The solutions belonging to the first subgroup, namely those involving the use of spectral analysis, are currently not developed. This type of parameter estimation was already investigated in the 1980s. The authors (Matsuo and Lipo, 1985) then used an additional negative-sequence current signal, detected the negative-sequence voltage, and calculated the value of the rotor resistance based on the obtained information.

A larger group are solutions based on state observers, and research on them is more relevant. In this case, we can distinguish two main methods: extended Kalman filter (EKF) (Zerdali and Barut, 2018) and extended Luenberger observer (ELO) (Orlowska-Kowalska, 1989). The research of Talla et al. (2015) presents EKF for estimating stator and rotor resistance for drives with an IM. This estimator was also implemented in the TMS320F28335 DSP processor, achieving satisfactory results. Another approach is to apply two EKF algorithms, one for stator resistance estimation and the other for estimation rotor resistance, which are switched during the system operation (Baghli et al., 2006). Demir et al. (2017) presented the EKF for estimating the rotor and stator resistances in the vector control structure. Also, a solution based on extended Luenberger-sliding mode observer (ELSMO) was proposed in Kim et al.'s study (2017). The advantage of ELO over EKF is that the performance of the observer can be increased by a simple adjusting of the gain matrix. The main problem of the observer-based techniques is their computational complexity, especially for EKF.

The most numerous subgroup consists of MRAS-type estimators. They use two models: adaptive and reference. Their responses are compared, and on this basis, the parameter of the adaptive model is adjusted so that its response is the same as that of the reference model. In this way, it is possible to estimate selected parameters of an IM. Kojabadi (2009) presents a solution based on the current model of the rotor flux. Zorgani et al. (2010, 2018) also proposed the MRAS for rotor resistance estimation, which can be implemented using both current and voltage models of the stator flux. On the other hand, in the research of Mapelli et al. (2012), a comparison of three estimation methods based on active and reactive power, as well as torque, was made. Another MRAS-type solution

is presented in Adamczyk's study (2020), where the stator current measurement was the reference model and the stator current estimator was the adaptive one.

The last group includes the remaining methods. It includes all solutions based on artificial neural networks (NNs). An example may be the study of Gonzalez et al. (2008), in which the applied offline trained NN consists of three layers: the first layer has 14 neurons, the hidden layer has 5 neurons, and the output layer has only 1 neuron, which is the unique output signal of the rotor resistance value. Another approach is a NN with a linear activation function that does not require offline learning. These are solutions using a reference model, similarly to the MRAS-type estimators, and an example can be found in the research of Karanayil et al. (2007). The method that does not use artificial intelligence is that of Toliyat et al. (1999). It requires neither a special test signal nor complicated calculations. It is based on a special voltage inverter key switching technique.

This paper presents an active CS-FTC strategy for the vector-controlled IM drive with a stator current estimator equipped with online adaptation of the rotor and stator resistance. The main objective of this article is to increase the accuracy of stator current estimation, which translates into precise detection and compensation in the event of a CS fault. The second section presents the mathematical model of IM, while the third section presents the model of the stator current estimator and the detection and compensation of CS fault based on this estimator. In the fourth section, the NN-based MRAS-type estimator for rotor resistance is described. Additionally, a proportional adaptation of the stator resistance is proposed based on the NN output. The fifth section presents a wide simulation analysis of the quality of stator current estimation in the case of rotor and stator resistance. The entire research is summarised in the final section.

2. Mathematical Model of IM

The implementation of the mathematical model of the IM requires the use of certain simplifications, described in more detail in Orlowska-Kowalska's study (2003). By using generalised space vectors, this model can be expressed in a stationary coordinate system (α–β), in relative quantities [p.u.], using the following equations:

- Voltage equation of the stator and rotor windings:

$$\frac{\mathrm{d}}{\mathrm{d}t}\mathbf{\Psi}_s = \left(\mathbf{u}_s - r_s\mathbf{i}_s\right)\frac{1}{T_N},\tag{1}$$

$$\frac{\mathrm{d}}{\mathrm{d}t}\mathbf{\Psi}_r = \left(\frac{r_r}{l_r}\left(l_m\mathbf{i}_s - \mathbf{\Psi}_r\right) + j\omega_m\mathbf{\Psi}_r\right)\frac{1}{T_N},\tag{2}$$

- Flux-current equations:

$$\mathbf{\Psi}_s = l_s\mathbf{i}_s + l_m\mathbf{i}_r,\tag{3}$$

$$\mathbf{\Psi}_r = l_r\mathbf{i}_r + l_m\mathbf{i}_s,\tag{4}$$

- Equation for IM electromagnetic torque:

$$t_{em} = \mathrm{Im}\left(\mathbf{\Psi}_s^*\mathbf{i}_s\right),\tag{5}$$

- Equation of motion:

$$\frac{\mathrm{d}}{\mathrm{d}t}\omega_m = \left(t_{em} - t_L\right)\frac{1}{T_M}.\tag{6}$$

where $l_r = l_{\sigma r} + l_m$, $l_s = l_{\sigma s} + l_m$, $T_N = 1/(2\pi f_{sN})$, and T_M represents the mechanical time constant.

3. CS-FTC

3.1. Stator current estimator

The stator current estimator is based on the virtual current sensor (VCS), shown in the study of Adamczyk and Orlowska-Kowalska (2019). The equation for stator current can be presented as follows:

$$\frac{d}{dt}\mathbf{i}_s^e = \frac{1}{l_s\sigma}\left(\mathbf{u}_s - r_s\mathbf{i}_s^e - T_N\frac{l_m}{l_r}\frac{d}{dt}\mathbf{\Psi}_r^i\right)\frac{1}{T_N},\tag{7}$$

where the current model of the rotor flux vector is used:

$$\frac{d}{dt}\mathbf{\Psi}_r^i = \left(\frac{r_r}{l_r}\left(l_m\mathbf{i}_s^e - \mathbf{\Psi}_r^i\right) - j\omega_m\mathbf{\Psi}_r^i\right)\frac{1}{T_N},\tag{8}$$

and stator voltage is calculated based on duty cycle values d_A, d_B, d_C, and u_{dc} voltage in the DC-link of VSI:

$$\begin{bmatrix} u_{s\alpha} \\ u_{s\beta} \end{bmatrix} = \frac{1}{3}\begin{bmatrix} 2d_A - d_B - d_C \\ \sqrt{3}\left(d_B - d_C\right) \end{bmatrix} u_{DC}.\tag{9}$$

The algorithm is mainly sensitive to changes in rotor resistance. Additionally, in the low angular velocity range, a significant effect of stator resistance can be observed (Adamczyk and Orlowska-Kowalska, 2022).

3.2. CS fault detection (CS-FD) and compensation

To realise the CS-FTC strategy, the calculation of phase current in *A* and *B* phases is necessary. Therefore, the (*a–b*) currents, calculated using VCS, are transformed according to:

$$\begin{bmatrix} i_{sA}^e \\ i_{sB}^e \end{bmatrix} = \frac{1}{2}\begin{bmatrix} 2 & 0 \\ -1 & \sqrt{3} \end{bmatrix}\begin{bmatrix} i_{s\alpha}^e \\ i_{s\beta}^e \end{bmatrix}.\tag{10}$$

The CS-FD is based on the square of the phase stator current estimation error in the *k*-th sample as:

$$\varepsilon_{A/B}(k) = \left(i_{sA/B}(k) - i_{sA/B}^e(k)\right)^2.\tag{11}$$

When the ε value for a given phase exceeds the adopted threshold value, ξ, for two consecutive samples, the λ coefficient changes from 0 to 1, as follows:

$$\lambda_{A/B}(k) = \begin{cases} 1 & \text{for} \quad \varepsilon_{A/B}(k) \geq \xi \quad \text{and} \quad \varepsilon_{A/B}(k-1) \geq \xi \\ 0 & \text{for} \quad \varepsilon_{A/B}(k) < \xi \quad \text{and} \quad \lambda_{A/B}(k-1) \neq 1 \end{cases}.\tag{12}$$

Finally, corrected currents (index *c*) are calculated based on estimated and actually available measured phase currents, as follows:

$$\begin{bmatrix} i_{s\alpha}^c \\ i_{s\beta}^c \end{bmatrix} = \frac{1}{\sqrt{3}}\begin{bmatrix} 1 & 0 \\ 1 & 2 \end{bmatrix}\begin{bmatrix} (1-\lambda_A)i_{sA} + \lambda_A i_{sA}^e \\ (1-\lambda_B)i_{sB} + \lambda_B i_{sB}^e \end{bmatrix}.\tag{13}$$

4. Rotor and Stator Resistance Adaptation

The solution presented in Ben-Brahim and Kurosawa (1993) shows a speed estimator based on the NN and MRAS concept. In this estimator, the authors assumed constant rotor resistance. However, this algorithm can be

transformed to estimate the rotor resistance in accompaniment with measurement of the rotor speed, as has been demonstrated in the research of Karanayil et al. (2007). To estimate the resistance of the rotor, a single-layer NN with a linear activation function is used. The solution is based on voltage (Eq. (14)) and current (Eq. (15)); Eq. (16) models the rotor flux in (α–β) frames, as in MRAS-type speed estimators.

The solution proposed in this paper is dedicated to CS-FTC systems and thus uses corrected currents (Eq. (13)) instead of measured currents. Therefore, the voltage model of the rotor flux used here as a reference model can be written as follows:

$$\frac{d}{dt}\boldsymbol{\Psi}_r^u = \frac{l_r}{l_m}\left(\mathbf{u}_s - r_s\mathbf{i}_s^c - \sigma l_s T_N \frac{d}{dt}\mathbf{i}_s^c\right)\frac{1}{T_N}. \tag{14}$$

The current model (Eq. (8)), which is used as an adaptive model, can, when presented in a discrete form, be written as:

$$\Psi_{r\alpha}^i(k+1) = W_1\Psi_{r\alpha}^i(k) - W_2\Psi_{r\beta}^i(k) + W_3 i_{s\alpha}^c, \tag{15}$$

$$\Psi_{r\beta}^i(k+1) = W_1\Psi_{r\beta}^i(k) + W_2\Psi_{r\alpha}^i(k+1) + W_3 i_{s\beta}^c, \tag{16}$$

where:

$$W_1 = 1 - \frac{T_S}{T_N}\frac{r_r}{l_r}, \quad W_2 = \frac{T_S}{T_N}\omega_m, \quad W_3 = \frac{T_S}{T_N}\frac{r_r l_m}{l_r}, \tag{17}$$

and T_s is the sampling time.

Eqs. (15) and (16) can be taken as a description of the recurrent NN with two neurons with linear activation functions. Two out of three weights of this NN, W_1 and W_3, are dependent on the rotor resistance. Resultantly, a simple transformation of these weights allows calculation of this parameter, as follows:

$$r_r^e = (1 - W_1)l_r\frac{T_S}{T_N}, \quad r_r^e = W_3\frac{l_r}{l_m}\frac{T_S}{T_N}. \tag{18}$$

As a result, it was decided to use the average value of both the calculated rotor resistance values.
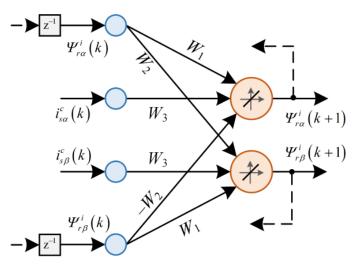
The NN described above is presented in Figure 1.

Fig. 1. NN based on the current model of rotor flux used in estimating the rotor resistance. NN, neural network.

The main idea for this solution relies on the change in NN weights W_1 and W_3, and minimisation of the difference between the adaptive (current) and reference (voltage) models is the aim of the solution, which can be realised by minimising the energy function, $\mathbf{E}(k)$, which is defined as follows:

$$\mathbf{E}(k) = \frac{1}{2}\left(\mathbf{\Psi}_r^u(k) - \mathbf{\Psi}_r^i(k)\right)^2 = \frac{1}{2}\left(\mathbf{e}_{\Psi}(k)\right)^2. \tag{19}$$

Next, the new weights are calculated as:

$$W_1(k+1) = W_1(k) + \eta \delta W_1(k), \tag{20}$$

$$W_3(k+1) = W_3(k) + \eta \delta W_3(k), \tag{21}$$

where:

$$\delta W_1(k) = \frac{\partial \mathbf{E}}{dW_1} = \left[\mathbf{\Psi}_r^u(k) - \mathbf{\Psi}_r^i(k)\right]^T \mathbf{I}\mathbf{\Psi}_r^i(k) = e_{\psi\alpha}\Psi_{r\alpha}^i + e_{\psi\beta}\Psi_{r\beta}^i, \tag{22}$$

$$\delta W_3(k) = \frac{\partial \mathbf{E}}{\partial W_3} = \left[\mathbf{\Psi}_r^u(k) - \mathbf{\Psi}_r^i(k)\right]^T \mathbf{I}\mathbf{i}_s^c(k) = e_{\psi\alpha}i_{s\alpha}^c + e_{\psi\beta}i_{s\beta}^c, \tag{23}$$

where $\mathbf{I} = \begin{bmatrix} 1 & 0 \\ 0 & 1 \end{bmatrix}$ and η is the training coefficient.

It should be noted that the changes in resistance values are dependent on the winding temperature. Thermal analysis carried out indicates that the temperature changes in the rotor cage and stator windings are similar and can reach up to 60°C (Badran et al., 2012). Typically, the rotor cage is made of aluminium, whereas the stator windings are made of copper. Both copper and aluminium have a similar temperature coefficient of resistance (TCR), which is around 0.004 K^{-1}. By substituting this value into the well-known relationship between resistance and temperature, it becomes evident that for $\Delta T = 60°C = 60$ K, the changes amount to 24%, as follows (Blasdel et al., 2014):

$$r_p = r_{pN}\left(1 + \Delta T \cdot TCR_{rp}\right) = r_{pN}\left(1 + 60 \cdot 0.004\right) = 1.24 r_{pN}, \; p \in \{r, s\}. \tag{24}$$

Therefore, in this article, when the rotor resistance is estimated using the proposed NN-MRAS-type model, the proportional change in the stator resistance has been assumed similarly as in the work of Kubota et al. (1993), as:

$$r_s^e = \frac{r_r^e}{r_{rN}} r_{sN}. \tag{25}$$

Thus, the overall scheme based on the NN of the rotor resistance estimation with proportional adaptation of the stator resistance is presented in Figure 2.
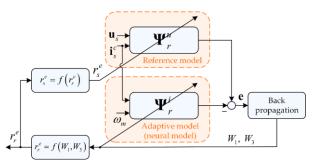

Fig. 2. The NN-based MRAS-type rotor resistance estimation with proportional adaptation of stator resistance. MRAS, model reference adaptive system; NN, neural network.

5. Simulation Tests

5.1. CS-FD and compensation

For simulation studies, the MATLAB/Simulink environment (by MathWorks, USA) was utilised and the calculations were performed using the ode1 method with a calculation step of 6.25e-6. The IM parameters are presented in Table A1 in Appendix. The direct rotor flux-oriented control (DRFOC) strategy was chosen for control of the IM drive. The overall CS-FTC control structure is presented in Figure 3.

In this article, based on thermal analysis (Badran et al., 2012), it was assumed that the changes in the resistance of the rotor and stator would be 25% and 30%, respectively, in the simulation studies. In the mathematical model, the resistances increased inertially from $t = 2$ s, according to the waveforms shown in Figure 4. It should be noted that the simulations did not take into account the actual thermal time constant of the motor in order to shorten the simulation time.
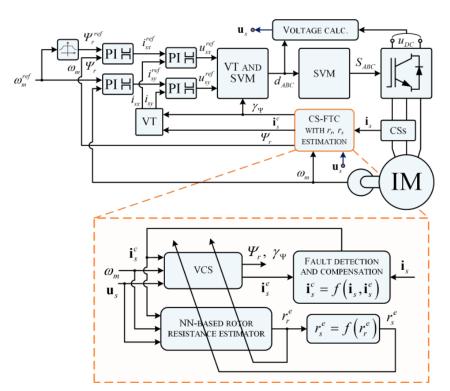

Fig. 3. The DRFOC control structure with the CS-FTC system and the estimation of rotor and stator resistances. CS, current sensor; DRFOC, direct rotor flux-oriented control; FTC, fault-tolerant control.
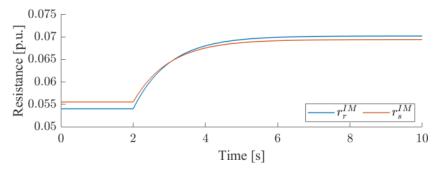

Fig. 4. Rotor and stator resistance changes assumed in the IM mathematical model. IM, induction motor.

The studies were carried out under steady-state and transient conditions.

- Steady-states: for two rotor speeds (100% and 10% of the rated value) and two load torques (25% and 75% of the rated load);
- Transient states: for rated speed and ±75% of the rated load (motoring and regenerative braking) shown in Figure 5a, and for ±100% of the rated speed and 75% of the rated load (from motoring to regenerating mode), as can be seen in Figure 5b.
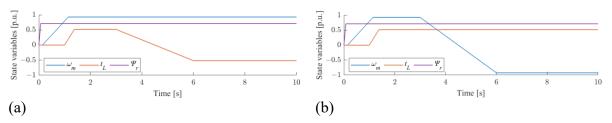

(a)   (b)

Fig. 5. Waveforms of the references speed, load, and rotor flux for regenerating mode under constant speed (a) and speed changes from motoring to regenerating mode (b).
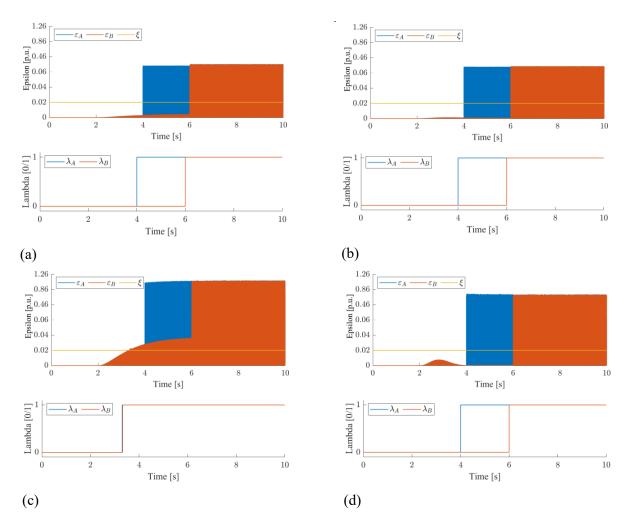

(a)   (b)

(c)   (d)

Fig. 6. Waveforms of λ and ε coefficients for the rated speed and: 25% of the rated load (a,b), 75% of the rated load (c,d); without (a,c) and with (b,d) estimation of the stator and rotor resistances.
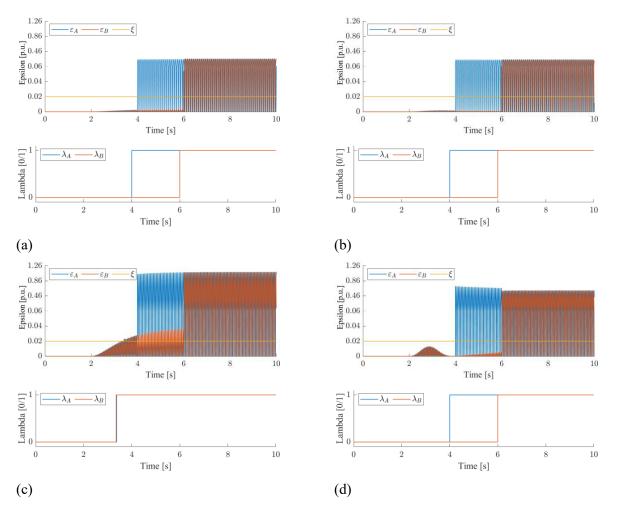
Fig. 7. Waveforms of ε and λ coefficients for 10% of the rated speed and: 25% of the rated load (a,b), 75% of the rated load (c,d); without (a,c) and with (b,d) estimation of the stator and rotor resistances.

The behaviour of the CS-FTC system was examined in the absence of rotor and stator resistance estimation, as well as with their estimation. The output of the rotor resistance estimator has been limited to the range of [0.5; 2.0] r_{rN}. The CS malfunction involved its complete disconnection: in phase A at $t = 4$ s and in phase B at $t = 6$ s. As there is no possibility for rotor resistance estimation in the MRAS system without phase current measurement, for all CS malfunctioning, the last known value of rotor resistance before the total CS malfunction is assumed. In these studies, the threshold ξ was taken as 0.02 [p.u], based on multiple simulation studies for the drive system. The accuracy of the CS-FD and compensation system was analysed in the conducted experiments without and with the estimation of both winding resistances.

5.2. FD tests

The quality of CS-FD was tested at the four operating points mentioned above, as well as for the inertia-driven changes in the stator and rotor resistances (see Figure 4). Figures 6–8 present graphs of the squared difference between the measured and estimated currents, according to Eq. (11), along with the waveforms of the λ coefficients, which determine the fault in a given phase.

To make the results more legible, two linear scales were used on the *y*-axis of the graphs that display the epsilon coefficients: one ranging from 0 to 0.06 with a step of 0.02, and the other ranging from 0.06 to 1.46 with a step of 0.4.
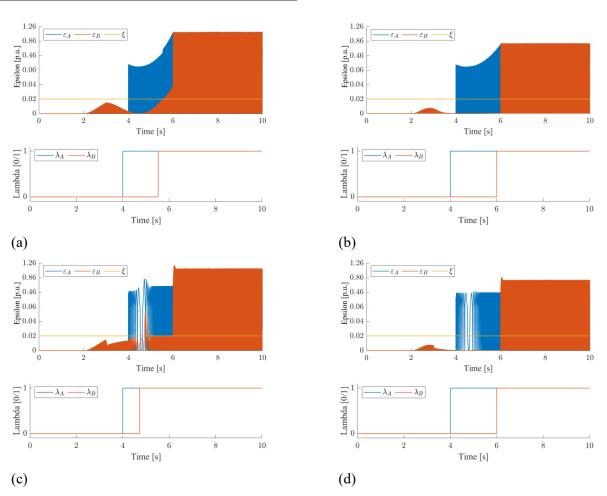
Fig. 8. Waveforms of ε and λ coefficients for: 100% of the rated speed and 75% of the rated load (regenerating mode) (a,b) and 100% of the rated speed (from motoring to regenerating mode) (c,d); without (a,c) and with (b,d) estimation of the stator and rotor resistances.

As can be seen in Figures 6 and 7, the estimation error squared largely depends on the degree to which the drive system is loaded. This is because the rotor resistance affects the current waveform when the system is loaded. At 75% of the rated torque, the system without rotor and stator resistance estimation (Figures 5c and 6c) is inaccurate and incorrectly signals a CS malfunction. Raising the threshold limit could decrease the accuracy of the fault detector.

Based on Figure 8, it can be observed that for transient states, the system correctly detected the first fault at $t = 4$ s, both in the case of estimating both resistances and without estimating the resistances. By applying parameter estimators, the system can adapt and compensate for changes in the system caused by faults. In this case, by estimating the IM parameters, the system was able to detect the second fault at $t = 6$ s correctly. Without estimation of the parameters, the system would not have been able to accurately identify the fault.

5.3. Quality of the stator and rotor resistances estimation
The quality of the estimation of the stator and rotor resistances was examined for the presented CS-FTC system. The obtained results are shown in Figures 9–11.

As can be seen, the quality of rotor and stator resistance estimation is much better for 75% of the rated torque (Figures 7c,d and 8c,d) than for 25% of the load (Figures 7a,b and 8a,b). However, in each of the obtained waveforms, the error in estimating these resistances did not exceed 20%, assuming initial changes of 25% for the
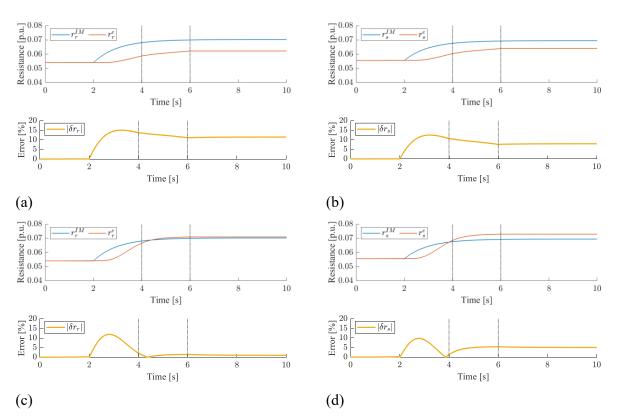
Fig. 9. Waveforms of both rotor and stator resistances for rated speed and: 25% of rated load (a,b), 75% of rated load (c,d); rotor resistance (a,c), stator resistance (b,d).
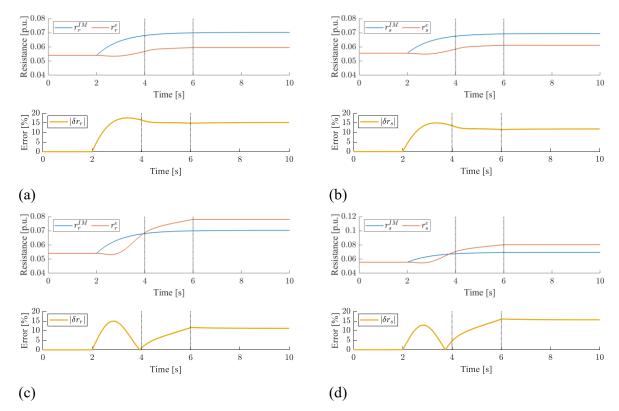

Fig. 10. Waveforms of both rotor and stator resistances for 10% of rated speed and: 25% of rated load (a,b), 75% of rated load (c,d); rotor resistance (a,c), stator resistance (b,d).
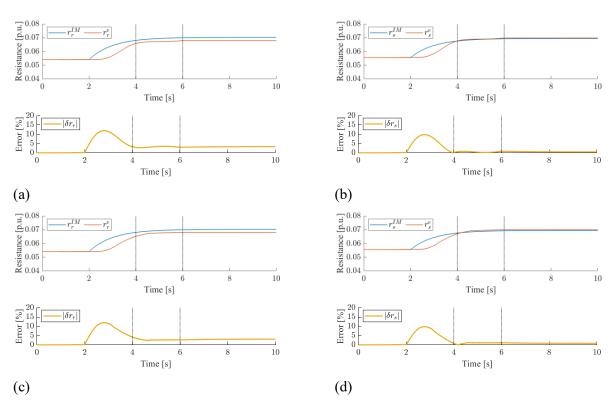
(a)

(b)

(c)

(d)

Fig. 11. Waveforms of both rotor and stator resistances for: 100% of the rated speed and 75% of the rated load (regenerating mode) (a,b) and 100% of the rated speed (from motoring to regenerating mode) (c,d); rotor resistance (a,c), stator resistance (b,d).

rotor resistance and 30% for the stator resistance. Furthermore, it should be emphasised that for the rated speed and 75% of the rated load, the final value of the error in estimating the rotor resistance was 1%, while for the stator resistance it was 5%.

The quality of resistance estimation was very high during the transient states, demonstrating the effectiveness of the presented method. Estimation errors for rotor resistance were less than 5% and for stator resistance, they were even less than 1%.

5.4. Quality of stator current estimation

The last tests focus on evaluating the accuracy of stator current estimation. Based on the assumptions presented above, the quality of stator current estimation was analysed in the α and β axes based on:

(1) the measured currents (blue colour), and
(2) the corrected currents (orange colour).

Since the CS failure resulted in a complete signal loss, the dashed lines indicate the current values in the α and β axes if the CS were not damaged. The results obtained are presented in Figures 12–14.

As can be seen in Figures 9 and 10, the quality of the stator current reconstruction improves after applying the rotor and stator resistance estimation. In the case of a load equal to 25% of the rated value, there is no significant effect of resistance changes on the stator current. High accuracy in estimating stator current can also be observed during transient states (Figure 14). In the case of estimating both resistances, the corrected currents closely match the measured currents. Tables 1 and 2 show the RMSE values of the current for the plots presented in Figures 12 and 13 (Table 1) and 14 (Table 2), as well as the percentage improvement in the quality of stator current estimation when resistances are estimated, compared with the situation where no parameter estimation is applied.
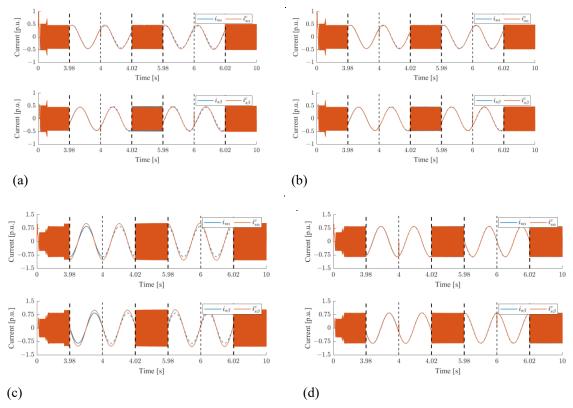
Fig. 12. Waveforms of α, β stator current components for the rated speed and: 25% of the rated load (a,b), 75% of the rated load (c,d); without (a,c) and with (b,d) estimation of the stator and rotor resistances.

Fig. 13. Waveforms of α, β stator current components for 10% of the rated speed and: 25% of the rated load (a,b), 75% of the rated load (c,d); without (a,c) and with (b,d) estimation of the stator and rotor resistances.
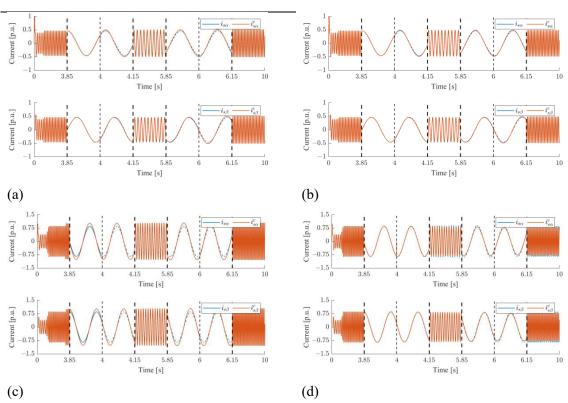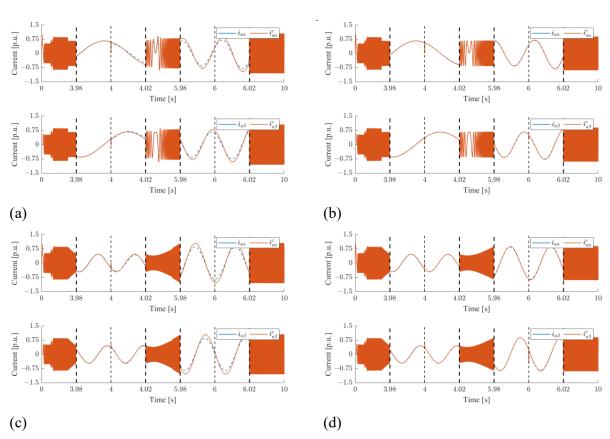
(a)

(b)

(c)

(d)

Fig. 14. Waveforms of α, β stator current components for 100% of the rated speed and 75% of the rated load (regenerating mode) (a,b) and 100% of the rated speed (from motoring to regenerating mode) (c,d); without (a,c) and with (b,d) estimation of the stator and rotor resistances.

The average RMSE value for the α–β stator current has been calculated for the period from $t_1 = 0$ s to $t_2 = 10$ s, as follows:

$$\Delta i_s = \frac{1}{2}\left(\sqrt{\frac{\sum_{k=t_1/T_s}^{t_2/T_s+1}\left(i_{s\alpha}(k)-i_{s\alpha}^c(k)\right)^2}{(t_2-t_1)/T_s+1}} + \sqrt{\frac{\sum_{k=t_1/T_s}^{t_2/T_s+1}\left(i_{s\beta}(k)-i_{s\beta}^c(k)\right)^2}{(t_2-t_1)/T_s+1}} \right),$$

(26)

where T_s is the sampling time.

	100% speed		10% speed	
	25% load	75% load	25% load	75% load
RMSE without resistance estimation	0.0329	0.1079	0.0282	0.1075
RMSE with resistance estimation	0.0147	0.0058	0.0166	0.0380
Percentage improvement	55.3	94.7	41.1	64.7

Table 1. RMSE values for reconstructed stator current, for steady states.

	Regenerative braking	Change of speed
RMSE without resistance estimation	0.0932	0.0983
RMSE with resistance estimation	0.0120	0.0113
Percentage improvement	87.1	88.5

Table 2. RMSE values for reconstructed stator current, for transient states.

As can be seen in Table 1, the improvement ranged from 41.1% for low rotor speed and light load to 94.7% for nominal speed and significant load (75% of the rated value). For transients, the improvement for regenerative braking was more than 87%, and for speed change it was more than 88% (Table 2). The conducted studies confirm the necessity of using rotor and stator resistance estimation in the case of CS-FTC-type systems.

6. Conclusions

The results of the study indicate that the quality of stator current reconstruction in the CS-FTC system can be significantly improved by implementing rotor and stator resistance adaptation in the proposed stator current estimator. The accuracy of the system largely depends on the load condition, and in the case of 75% of the rated load or higher, the estimation error for the rotor resistance was as low as 1% and for the stator resistance it was in the range of 5%. The improvement in the quality of stator current estimation ranged from 41.1% to 94.7% for steady states (depending on the motor operating point) and from 87.1% to 88.5% for transients, when resistance estimation was applied. It should be emphasised, however, that drive systems are designed to operate at or near rated operating points, and it is in such a situation that the greatest improvement (94.7%) was observed. In addition, the applied solution significantly improves the quality of stator current estimation in transients, resulting in high-quality correct FD. These findings highlight the importance of resistance estimation in CS-FTC systems and provide information on the design and implementation of more accurate and reliable control systems for electrical drives.

Acknowledgment

References

Adamczyk, M. (2020). Rotor Resistance Estimator based on Virtual Current Sensor Algorithm for Induction Motor Drives. *Power Electronics and Drives*, 5(40), pp. 143–156.

Adamczyk, M. and Orlowska-Kowalska, T. (2019). Virtual Current Sensor in the Fault-Tolerant Field-Oriented Control Structure of an Induction Motor Drive. *Sensors*, 19(22), p. 4979.

Adamczyk, M. and Orlowska-Kowalska, T. (2021). Current sensors fault detection and tolerant control for induction motor drive. In: *2021 IEEE 19th International Power Electronics and Motion Control Conference (PEMC)*, 25–29 April 2021, Gliwice, Poland, pp. 888–892.

Adamczyk, M. and Orlowska-Kowalska, T. (2022). Postfault Direct Field-Oriented Control of Induction Motor Drive using Adaptive Virtual Current Sensor. *IEEE Transactions on Industrial Electronics*, 69(4), pp. 3418–3427.

Azzoug, Y., Sahraoui, M., Pusca, R., Ameid, T., Romary, R. and Cardoso, A. J. M. (2021). High-performance Vector Control without AC Phase Current Sensors for Induction Motor Drives: Simulation and Real-Time Implementation. *ISA Transactions*, 109, pp. 295–306.

Badran, O., Sarhan, H. and Alomour, B. (2012). Thermal Performance Analysis of Induction Motor. *International Journal of Heat and Technology*, 30(1), pp. 75–88.

Baghli, L., Al-Rouh, I. and Rezzoug, A. (2006). Signal Analysis and Identification for Induction Motor Sensorless Control. *Control Engineering Practice*, 14(11), pp. 1313–1324.

Ben-Brahim, L. and Kurosawa, R. (1993). Identification of induction motor speed using neural networks. In: *Conference Record of the Power Conversion Conference-Yokohama 1993*, 19–21 April 1993, Yokohama, Japan, pp. 689–694.

Blasdel, N. J., Wujcik, E. K., Carletta, J. E., Lee, K. S. and Monty, C. N. (2014). Fabric Nanocomposite Resistance Temperature Detector. *IEEE Sensors Journal*, 15(1), pp. 300–306.

Demir, R., Barut, M., Yildiz, R., Inan, R. and Zerdali, E. (2017). EKF based rotor and stator resistance estimations for direct torque control of induction motors. In: *2017 International Conference on*

Optimization of Electrical and Electronic Equipment (OPTIM) & 2017 Intl Aegean Conference on Electrical Machines and Power Electronics (ACEMP), 25–27 May 2017, Brasov, Romania, pp. 376–381).

Gonzalez, H., Rivas, R. and Rodriguez, T. (2008). Using an Artificial Neural Network as a Rotor Resistance Estimator in the Indirect Vector Control of an Induction Motor. *IEEE Latin America Transactions*, 6(2), pp. 176–183.

Jankowska, K. and Dybkowski, M. (2022). Design and Analysis of Current Sensor Fault Detection Mechanisms for PMSM Drives based on Neural Networks. *Designs*, 6(1), p. 18.

Karanayil, B., Rahman, M. F. and Grantham, C. (2007). Online Stator and Rotor Resistance Estimation Scheme using Artificial Neural Networks for Vector Controlled Speed Sensorless Induction Motor Drive. *IEEE Transactions on Industrial Electronics*, 54(1), pp. 167–176.

Kim, J., Ko, J., Lee, J. and Lee, Y. (2017). Rotor Flux and Rotor Resistance Estimation using Extended Luenberger-Sliding Mode Observer (ELSMO) for three Phase Induction Motor Control. *Canadian Journal of Electrical and Computer Engineering*, 40(3), pp. 181–188.

Kojabadi, H. M. (2009). Active Power and MRAS based Rotor Resistance Identification of an IM Drive. *Simulation Modelling Practice and Theory*, 17(2), pp. 376–389.

Kubota, H., Matsuse, K. and Nakano, T. (1993). DSP-based Speed Adaptive Flux Observer of Induction Motor. *IEEE Transactions on Industry Applications*, 29(2), pp. 344–348.

Mapelli, F. L., Bezzolato, A. and Tarsitano, D. (2012). A rotor resistance MRAS estimator for induction motor traction drive for electrical vehicles. In: *2012 XXth International Conference on Electrical Machines*, 02–05 September 2012, Marseille, France, pp. 823–829.

Matsuo, T. and Lipo, T. A. (1985). A Rotor Parameter Identification Scheme for Vector-Controlled Induction Motor Drives. *IEEE Transactions on Industry Applications*, IA-21(3), pp. 624–632.

Najafabadi, T. A., Salmasi, F. R. and Jabehdar-Maralani, P. (2010). Detection and Isolation of Speed-, DC-Link Voltage-, and Current-Sensor Faults based on an Adaptive Observer in Induction-Motor Drives. *IEEE Transactions on Industrial Electronics*, 58(5), pp. 1662–1672.

Orlowska-Kowalska, T. (1989). Application of Extended Luenberger Observer for Flux and Rotor Time-Constant Estimation in Induction Motor Drives. *IEE Proceedings D (Control Theory and Applications),* 136(6), pp. 324–330.

Orlowska-Kowalska, T. (2003). *Sensoless Induction Motor Drives*. Wrocław: Wroclaw University of Technology Press.

Salmasi, F. R. (2017). A Self-Healing Induction Motor Drive with Model Free Sensor Tampering and Sensor Fault Detection, Isolation, and Compensation. *IEEE Transactions on Industrial Electronics*, 64(8), pp. 6105–6115.

Shi, X. and Krishnamurthy, M. (2014). Survivable Operation of Induction Machine Drives with Smooth Transition Strategy for EV Applications. *IEEE Journal of Emerging and Selected Topics in Power Electronics*, 2(3), pp. 609–617.

Talla, J., Peroutka, Z., Blahnik, V. and Streit, L. (2015). Rotor and stator resistance estimation of induction motor based on augmented EKF. In: *2015 International Conference on Applied Electronics (AE)*, 08–09 September 2015, Pilsen, Czech Republic, pp. 253–258.

Toliyat, H. A., Arefeen, M. S., Rahman, K. M. and Figoli, D. (1999). Rotor Time Constant Updating Scheme for a Rotor Flux-Oriented Induction Motor Drive. *IEEE Transactions on Power Electronics*, 14(5), pp. 850–857.

Toliyat, H. A., Levi, E. and Raina, M. (2003). A Review of RFO Induction Motor Parameter Estimation Techniques. *IEEE Transactions on Energy Conversion*, 18(2), pp. 271–283.

Zerdali, E. and Barut, M. (2018). Extended Kalman Filter Based Speed-Sensorless Load Torque and Inertia Estimations with Observability Analysis for Induction Motors. *Power Electronics and Drives*, 3(38), pp. 115–127.

Zorgani, Y. A., Jouili, M., Koubaa, Y. and Boussak, M. (2018). A Very-Low-Speed Sensorless Control Induction Motor Drive with Online Rotor Resistance Tuning by using MRAS Scheme. *Power Electronics and Drives*, 4(1), pp. 125–140.

Zorgani, Y. A., Koubaa, Y. and Boussak, M. (2010). Simultaneous estimation of speed and rotor resistance in sensorless ISFOC induction motor drive based on MRAS scheme. In: *The XIX International Conference on Electrical Machines-ICEM 2010*, 06–08 September 2010, Rome, Italy, pp. 1–6.

Appendix

Symbol	[PH.U.]	[p.u.]
Rated phase voltage, U_N	230 V	0.707
Rated phase current, I_N	2.5 A	0.707
Rated power, P_N	1.1 kW	0.638
Rated speed, n_N	1390 rpm	0.927
Rated torque, T_{eN}	7.56 Nm	0.688
Number of pole pairs, p_b	2	-
Rotor winding resistance, R_r	4.968 Ω	0.0540
Stator winding resistance, R_s	5.114 Ω	0.0556
Rotor leakage inductance, $L_{\sigma r}$	31.6 mH	0.1079
Stator leakage inductance, $L_{\sigma s}$	31.6 mH	0.1079
Main inductance, L_m	541.7 mH	1.8498
Rated rotor flux, Ψ_{rN}	0.7441 Wb	0.7187
Rated stator flux, Ψ_{sN}	0.8235 Wb	0.7954
Mechanical time constant, T_M	0.25 s	-

Table A1. Rated parameters of the tested IM.